Fast Lumped Parameter Identification of Linear EMVEH Based on Thevenin Equivalent Measurement and Five-Point Extraction Algorithm

Huakang Xia, Yinshui Xia, Libo Qian, *Member, IEEE*, Ge Shi, *Senior Member, IEEE*, Zhidong Chen, and Xiudeng Wang, *Member, IEEE*

***Abstract*—The lumped parameter model of linear electromagnetic vibration energy harvester (EMVEH) is commonly employed, however, identifying the model parameters is a tedious task. Therefore, this article proposes a fast-lumped parameter identification method for linear EMVEHs. The proposed method only requires Thevenin equivalent measurement to prepare the original data, including open-circuit voltage and output impedance. It is mainly based on electrical measurement and does not require a laser vibrometer. Also, a five-point extraction algorithm is introduced to explore the information of parameters from the impedance data. It is analytical rather than simple curve fitting. The theoretical derivations, proof of principle, and simulation of the method are fully presented. In addition, the experimental validations are also performed on an unpackaged and another packaged EMVEH prototype, which can confirm the feasibility of the proposed method. Compared with existing methods, the proposed method not only can achieve the same test accuracy, but also can offer high technical applicability, and operation convenience, which can be applied to packaged EMVEHs and rapid measurement in the industrial field.**

***Index Terms*—Analytical solution, electromagnetic vibration energy harvester (EMVEH), five-point extraction algorithm, lumped-parameter model, parameter identification, Thevenin equivalent measurement.**

Received 6 February 2024; revised 1 June 2024 and 18 July 2024; accepted 24 August 2024. Date of publication 29 August 2024; date of current version 7 October 2024. This work was supported in part by the National Key R&D Program of China under Grant 2022YFB4401000, in part by the National Natural Science Foundation of China under Grant 62271275, Grant 62131010, Grant U22A2013, Grant 61971389, and Grant 62222406, in part by the Natural Science Foundation of Zhejiang Province under Grant LR22F010001 and Grant LDT23F04022F04, in part by the Natural Science Foundation of Ningbo under Grant 2023J122 and Grant 2021J058, and in part by the K.C. Wong Magna Fund in Ningbo University. Recommended for publication by Associate Editor M. Vitelli. *(Corresponding author: Libo Qian.)*

Huakang Xia and Yinshui Xia are with the Faculty of Electrical Engineering and Computer Science, Ningbo University, Ningbo 315211, China (e-mail: xiahuakang@nbu.edu.cn; xiayinshui@nbu.edu.cn).

Libo Qian and Xiudeng Wang are with the Key Laboratory of Analog Integrated Circuits, and Hangzhou Institute of Technology, Xidian University, Xi'an 710071, China (e-mail: qianlibo@xidian.edu.cn; 1611082572@nbu.edu.cn).

Ge Shi is with the College of Mechanical and Electrical Engineering, China Jiliang University, Hangzhou 310018, China (e-mail: shige@cjlu.edu.cn).

Zhidong Chen is with the College of Information and Intelligence Engineering, Zhejiang Wanli University, Ningbo 315100, China (e-mail: 1701082016@nbu.edu.cn).

Color versions of one or more figures in this article are available at https://doi.org/10.1109/TPEL.2024.3451485.

Digital Object Identifier 10.1109/TPEL.2024.3451485

I. Introduction

AMBIENT vibration energy harvesting (VEH) is a promising technique to provide sustainable energy for autonomous microelectronic devices, such as wireless sensor nodes [1]. A typical VEH system consists of a front-end energy harvester and a back-end interface circuit. The energy harvester is responsible for converting vibrational energy into electrical energy, usually based on piezoelectric [2], electromagnetic [3], electrostatic [4], triboelectric [5], etc. The interface circuit is used to transfer the converted energy to the load, and it usually requires a special design according to the front end. Therefore, it is important to master a good understanding of the energy harvester's characteristics. In addition, a suitable harvester model is helpful for system simulation and performance estimation at the design stage [6], [7], [8], [9], [10].

The electromagnetic vibration energy harvester (EMVEH) is based on Faraday's law of electromagnetic induction, and is composed of magnets and coils. Various EMVEHs have been designed to improve performance metrics including power density and frequency response [11]. The linear EMVEH possess advantages, such as simple structure, reliable operation, and predictable behavior, making it widely adopted in practical applications [12], [13], [14]. Fig. 1(a) shows a linear cantilever-based EMVEH. According to the lumped parameter model theory, such an EMVEH can be expressed as a single-degree-of-freedom second-order damped vibration system [3], as shown in Fig. 1(b). This model is commonly used in the field of linear EMVEH and is suitable for system-level analysis, simulation, and circuit design [15], [16], [17], [18], [19], [20].

In general, only six global lumped parameters as listed in Table I are required to describe this model [21], [22]. According to their physical definition, they can be determined by various theoretical and experimental methods. Researchers in different fields can do this by using a preferred combination of operations [21], [22], [23], [24], [25]. Since these methods are not fully documented, they are collectively referred to herein as "traditional method." To the best of the author's knowledge, a typical procedure of the traditional method can be summarized as follows [21], [22], [25].

1) Identify the mechanical parameters M, D, and K through static and dynamic testing under appropriate electrical constraints.

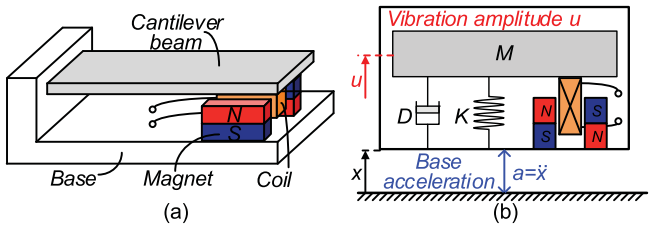

Fig. 1. (a) Linear cantilever-based EMVEH. (b) Equivalent dynamic model.

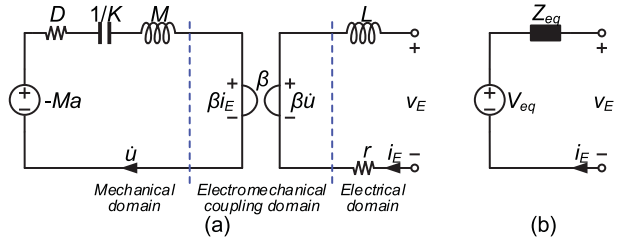

Fig. 2. (a) Equivalent circuit of EMVEH. (b) Thevenin equivalent circuit.

TABLE I
LUMPED PARAMETERS OF A LINEAR EMVEH

Parameters	Description	Unit (SI)
M	Modal mass	kg
D	Damper coefficient	N·s/m
K	Spring stiffness	N/m
r	Coil resistance	Ω
L	Coil inductance	H
β	Electromagnetic force–current factor	N/A

2) Measure the electrical parameters r and L by using an inductance-capacitance-resistance *(LCR)* meter or an impedance analyzer under appropriate mechanical constraints.
3) Calculate the electromagnetic force–current factor β by dividing the induced electromagnetic voltage by the relative vibration velocity of the mass.

It is acknowledged that the traditional method can work well in most cases. However, it involves specialized instrumentation and test methods, requiring the conversion of data collected from multiple sources, which is time-consuming and confusing [21]. In addition, it is difficult to apply mechanical constraints and laser vibrometers to a packaged EMVEH for specific measurements [13], [21], [25]. Without these treatments, parameter identification may become difficult. Although these treatments can be performed more easily by disassembling the packaged EMVEH, this operation may affect the magnetic field region, inductance measurement, functional and structural integrity, etc.

Several attempts have been made to accelerate and simplify the parameter identification process. Elvin and Elvin [24] proposed a relatively simple computational approach for calculating the electromechanical parameters of a linear EMVEH. Compared with the measured values, the calculated errors of coil resistance and inductance are $+5.8\%$ and -10%, respectively. In additional, some pretested experimental data still need to be substituted in the calculation process. Balato et al. [26] presented a method that utilizes the power versus frequency curve to determine the lumped parameters. This method offers convenience when the manufacturer has provided the necessary information about the EMVEH, otherwise, it still requires users to design the optimal load and measure the load power. Yuan et al. [27] developed a workflow to extract an "equivalent circuit" of EMVEH from a finite element model (FEM) built in ANSYS Maxwell 3-D. However, this so-called "equivalent circuit" is only a look-up table, not an explicit electrical model. Furthermore, simulation results still need to be verified experimentally in critical applications.

With the application of VEH technology, most commercial EMVEHs have appeared, such as PMG17 (Perpetuum Ltd.) [28], VEG-20/30/50/60/70 (XIDAS IoT) [29], and VEH-450 (Ferro Solutions) [30]. However, manufacturers only provide basic information, such as maximum output voltage, output power, and output impedance. The detailed parameters for estimating the electromechanical behaviors of EMVEH are not fully available. In addition, the above EMVEHs are all fully packaged devices, which poses a challenge to lumped parameter identification.

Therefore, the article proposes a fast-lumped parameter identification method for linear EMVEHs. This method relies mainly on electrical measurement and does not require laser vibrometers, mechanical constraints, and cumbersome operations. It only requires Thevenin equivalent measurement on a linear EMVEH to prepare the original data, including open-circuit voltage and output impedance tests. In addition, a five-point extraction algorithm is proposed to extract the information about the lumped parameters from the impedance data. Therefore, it is easier to implement and more suitable for packaged EMVEHs and industrial field measurements.

II. REVIEW OF EXISTING KNOWLEDGE

A. Theory of Linear EMVEH

The second-order spring-damper-mass vibration system depicted in Fig. 1(b), corresponding to a linear single degree-of-freedom (SDOF) EMVEH, can be further represented by an electrical circuit model [9], [21], [23], as shown in Fig. 2(a). The electromagnetic force–current factor β is modeled as a gyrator electrically. Accordingly, the electromechanical coupling equations for this system can be expressed as (1) and (2). The mechanical variables a and u represent the base acceleration excitation and displacement response, respectively. Also, the electrical variables v_E and i_E denote the electromagnetic output voltage and current, respectively. The descriptions of the remaining parameters have been presented in Table I

$$M\frac{d^2u}{dt^2} + D\frac{du}{dt} + Ku + \beta i_E = -Ma \tag{1}$$

$$v_E = \beta\frac{du}{dt} - L\frac{di_E}{dt} - ri_E. \tag{2}$$

B. Traditional Method

The traditional identification method is based on physical definitions of the lumped parameters. The brief principles and operations can be concluded as follows.

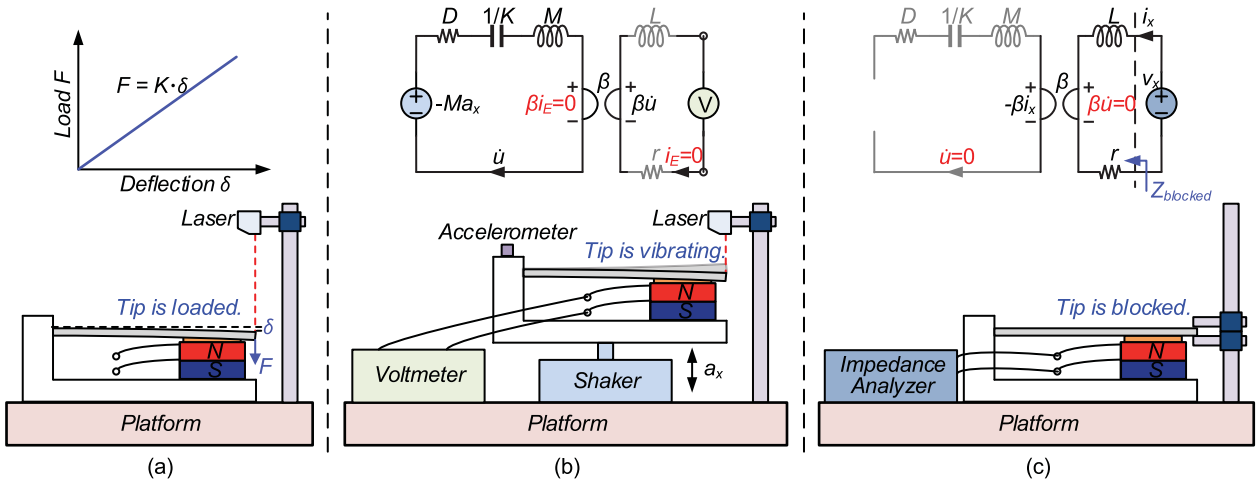

Fig. 3. Traditional method. (a) Setup for testing K. (b) Setup for testing M, D, and β. (c) Setup for testing r and L.

1) Identification of Parameters M, D, and K: The stiffness K can be measured by a static loading test on the spring component of the EMVEH as shown in Fig. 3(a). When the tip of the cantilever beam is subjected to a load F, it can produce a deflection δ. According to Hooke's Law, the stiffness K can be calculated as the load versus deflection as given by

$$K = \frac{F}{\delta}. \tag{3}$$

The setup shown in Fig. 3(b) can be used for testing M and D. The EMVEH is open-circuited and excited sinusoidally by a shaker. The base acceleration a_x is measured using an accelerometer. Meanwhile, the vibration amplitude u_m of the tip of the cantilever beam is measured by a laser vibrometer. Based on (1), the relation between a_x and u_m is derived as (4). Note that ω is the angular frequency of electrical signals in the equivalent circuit of EMVEH. Usually, a correction factor μ is used to compensate for the difference between the experiment and theory. Finally, the values of M and D can be solved by parametric curve fitting

$$u_m = \frac{\mu M a_x}{\sqrt{\left(K - \omega^2 M\right)^2 + \left(\omega D\right)^2}}. \tag{4}$$

2) Identification of Parameters r and L: The setup shown in Fig. 3(c) can be employed for measuring r and L. In order to avoid the influence of mechanical motion on electrical measurement, the cantilever beam is mechanically blocked in the test (u=0, $\dot{u}$=0) [21]. Thus, the mechanical domain of the EMVEH equivalent circuit is open-circuited. Then, the remaining circuit only including r and L can be easily measured using an impedance analyzer. The corresponding electrical impedance of the EMVEH in this mechanically blocked condition is given by

$$Z_{\text{blocked}}\left(\omega\right) = r + j\omega L. \tag{5}$$

3) Identification of Parameter β: The identification of β is also based on the setup shown in Fig. 3(b). A voltmeter is employed for measuring the open-circuit voltage V_E^{oc} of the EMVEH under a sinusoidal acceleration excitation. Since i_E is zero in (2) when the EMVEH is open-circuited, the expression of β is simplified to the ratio of open-circuit voltage to vibration velocity. The latter is further derived from the vibration amplitude u_m measured by a laser vibrometer. Therefore, the electromagnetic force-current factor β is calculated by

$$\beta = \frac{V_E^{\text{oc}}}{\omega u_m}. \tag{6}$$

The above operations show that the traditional method can always work with the help of specific constraints and laser vibrometers. However, it is difficult to apply these treatments to a packaged EMVEH for specific measurements. Also, the operations of traditional methods are still time-consuming and troublesome.

III. Proposed Parameter Identification Method

A. Thevenin Equivalent Circuit

Under the sinusoidal steady-state condition with an angular frequency ω, the Thevenin equivalent circuit can be derived as shown in Fig. 2(b). Furthermore, the Thevenin voltage $V_{\text{eq}}(\omega)$ and impedance $Z_{\text{eq}}(\omega)$ are calculated as (7) and (8), respectively. It is mathematically possible to determine these parameters by solving enough equations with different angular frequencies. However, it is inefficient and lacks interpretability. Instead, the proposed method determines these parameters by exploiting the intrinsic characteristics of these equations

$$V_{\text{eq}}\left(\omega\right) = \frac{-j\omega\beta M A\left(\omega\right)}{K - \omega^2 M + j\omega D} \tag{7}$$

$$Z_{\text{eq}}\left(\omega\right) = \frac{j\omega\beta^2}{K - \omega^2 M + j\omega D} + j\omega L + r. \tag{8}$$

Before explaining the proposed method, some intermediate parameters including ω_n, ζ_m, and k_e are introduced [25]. In fact, these parameters are commonly mentioned in the field of mechanics. The natural frequency ω_n, defined as $\sqrt{K/M}$, corresponds to the mechanical resonance frequency of the EMVEH

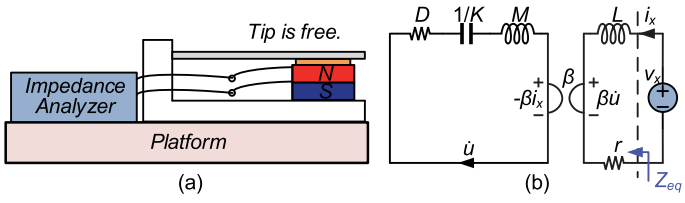

Fig. 4. Proposed method. (a) Setup for output impedance test. (b) Equivalent test circuit.

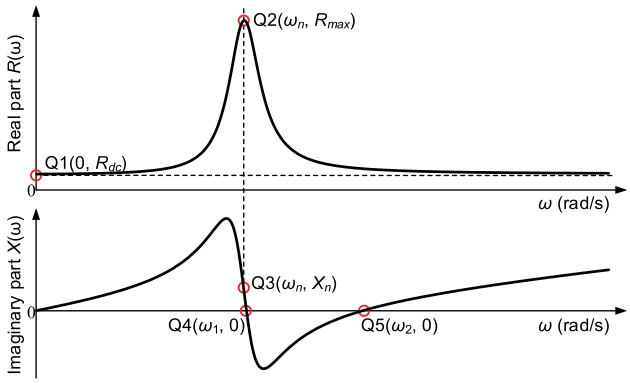

Fig. 5. Typical curves of real part $R(\omega)$ and imaginary part $X(\omega)$.

when it is open-circuited (i_E=0). The mechanical damping ratio ζ_m, defined as $D/(2M\omega_n)$, is usually small ($\zeta_m \ll 1$). The electromechanical coupling coefficient k_e, defined as $\beta/\sqrt{KL}$, is preferred to be large in a well-designed prototype. The proposed method requires two tests including output impedance test and open-circuit voltage test.

B. Output Impedance Test

The setup for the output impedance test in this method is different from that of the traditional method. As shown in Fig. 4, the tip of the cantilever beam is free rather than mechanically blocked. This means that no specific mechanical constraints are required and thus this test can be performed on a packaged EMVEH. In addition, the circuit of the mechanical domain is closed rather than open. Thus, the output impedance $Z_{\text{eq}}(\omega)$ measured in this mechanically free condition includes both the mechanical and electrical components.

Substitute the intermediate parameters into (8), then separate the real part $R(\omega)$ and imaginary part $X(\omega)$, respectively, as given by (9) and (10). The typical curves of $R(\omega)$ and $X(\omega)$ are plotted in Fig. 5. There are five key points located in the two curves, as denoted by Q_1–Q_5, which can be used for fast parameter identification. The proposed five-point extraction algorithm is explained as follows:

$$R(\omega) = \frac{2\zeta_m k_e^2 \omega_n^3 \omega^2 L}{\left(\omega_n^2 - \omega^2\right)^2 + \left(2\zeta_m \omega_n \omega\right)^2} + r \tag{9}$$

$$X(\omega) = \frac{\left(\omega_n^2 - \omega^2\right) k_e^2 \omega_n^2 \omega L}{\left(\omega_n^2 - \omega^2\right)^2 + \left(2\zeta_m \omega_n \omega\right)^2} + \omega L. \tag{10}$$

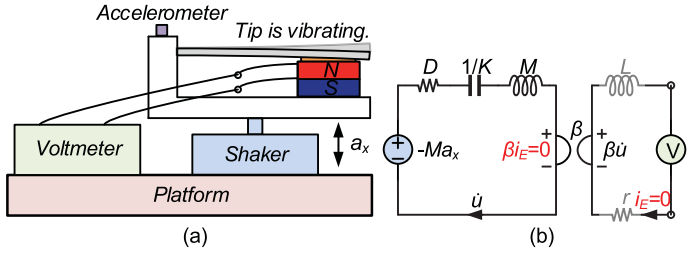

Fig. 6. Proposed method. (a) Setup for open-circuit voltage test. (b) Equivalent test circuit.

The first key point $Q_1(0, R_{\text{dc}})$ is the intersection between the $R(\omega)$ curve and the vertical axis, which is obtained by setting ω to zero or infinity in (9). Then, the coil resistance r is determined as follows:

$$r = R(0) = R(\infty) = R_{\text{dc}}. \tag{11}$$

The second key point $Q_2(\omega_n, R_{\text{max}})$ is actually the peak point of the $R(\omega)$ curve. It is obtained by setting ω to ω_n in (9). Also, if the remaining parameters are determined, the expression of R_{max} given in the following equation can be used to calculate the coil inductance L:

$$R_{\text{max}} = R(\omega_n) = \frac{k_e^2 \omega_n L}{2\zeta_m} + r. \tag{12}$$

Based on the value of ω_n read from Q_2, the third key point $Q_3(\omega_n, X_n)$ can be located in the $X(\omega)$ curve. The expression of X_n is derived from (10), as given in the following, which can be also used to calculate the coil inductance L:

$$X_n = X(\omega_n) = \omega_n L. \tag{13}$$

The remaining two key points are the nonzero intersections between the $X(\omega)$ curve with the horizontal axis, as marked by $Q_4(\omega_1, 0)$ and $Q_5(\omega_2, 0)$. Substitute ω_1 and ω_2 into (10), then ζ_m and k_e can be solved analytically as follows:

$$\zeta_m = \frac{\sqrt{\left(\omega_1^2 - \omega_n^2\right)\left(\omega_2^2 - \omega_n^2\right)}}{2\omega_n^2} \tag{14}$$

$$k_e = \frac{\sqrt{\omega_1^2 \omega_2^2 - \omega_n^4}}{\omega_n^2}. \tag{15}$$

C. Open-Circuit Voltage Test

So far, the parameters r, L, ω_n, ζ_m, and k_e have been obtained, while the remaining parameters M, D, K, and β are still undetermined. Fortunately, once any one of them is determined, all the others can be obtained together. Thus, another open-circuit voltage test is required to determine the parameter β. The corresponding setup and equivalent test circuit are presented in Fig. 6. Given the base acceleration a_x of $A_x \sin \omega_x t$ with an amplitude A_x and angular frequency ω_x, the open-circuit voltage $V_E^{\text{oc}} \sin(\omega_x t + \varphi_x)$ with an amplitude V_E^{oc} and initial phase φ_x can be observed. Then, based on (7), the parameter β can be

TABLE II
FORMULAS FOR CALCULATING LUMPED PARAMETERS

Parameter	Calculation	Parameter	Calculation
r	Eq.(11)	β	Eq.(16) or (17)
L	Eq.(12) or (13)	M	$\beta^2/\left(\omega_n^2 k_e^2 L\right)$
ζ_m	Eq.(14)	D	$2\zeta_m\beta^2/\left(\omega_n k_e^2 L\right)$
k_e	Eq.(15)	K	$\beta^2/\left(k_e^2 L\right)$

calculated as follows:

$$\beta = \frac{\sqrt{\left(\omega_n^2 - \omega_x^2\right)^2 + \left(2\zeta_m\omega_n\omega_x\right)^2}}{\omega_x}\frac{V_E^{\text{oc}}}{A_x}. \tag{16}$$

Because the electromechanical coupling dynamics test is involved, it is better to measure open-circuit voltage under different accelerations and frequencies in order to improve test accuracy. Then, the determination of β is considered as an optimization problem as described by

$$\beta = \arg\min_{(\beta)} \sum_{i=1}^{N} \left(V_{E,i}^{\text{oc}} - \frac{\omega_i \beta A_i}{\sqrt{\left(\omega_n^2 - \omega_i^2\right)^2 + \left(2\zeta_m\omega_n\omega_i\right)^2}} \right)^2 \tag{17}$$

where N represents the number of measurements. ω_i, A_i, and $V_{E,i}^{\text{oc}}$ are the angular frequency, acceleration amplitude, and open-circuit voltage in the ith measurement, respectively. Such an optimization problem can be easily solved by using numerical methods. Since β is determined, all the other parameters can be obtained subsequently. The involved formulas for calculation are summarized in Table II.

D. Proof of Principle

The existence of $Q_4(\omega_1, 0)$, $Q_5(\omega_2, 0)$, and the validity of (14) and (15) are not proved in the above derivation. Here, a loose proof of principle is presented as follows. The analytical solution of ω_1 and ω_2 is given by (18). As a thumb of rule, ζ_m is usually much less than unity. Also, the value of $k_e^2/(2\zeta_m)$ is usually large in a well-designed EMVEH, which can reach tens, hundreds or even thousands [25]. Thus, the condition of $k_e^2/(2\zeta_m) > 2\zeta_m + 2$ can be satisfied with a high probability, so does the existence of (18). Since $(k_e^2 - 4\zeta_m^2) > 4\zeta_m$ is valid, ω_n must be smaller than ω_1 and ω_2, which confirms the validity of (14) and (15). Finally, the validity of the proposed five-point extraction algorithm is guaranteed in most practical EMVEH prototypes

$$\omega_{1,2} = \omega_n \sqrt{1 + \frac{k_e^2 - 4\zeta_m^2 \pm \sqrt{\left(k_e^2 - 4\zeta_m^2\right)^2 - 16\zeta_m^2}}{2}}. \tag{18}$$

IV. SIMULATION TESTS

In order to verify the effectiveness of the proposed parameter identification method, the first simulation test is carried out using the electrical simulation data generated by LTspice. The equivalent circuit of a linear EMVEH is built in LTspice with the simulated parameters: M=50 g, D=1.5 N · s/m, K=5000 N/m, r=25 Ω, L=15 mH, and β=10 N/A. It is noted that the simulated circuit is an equivalent transformation of the circuit

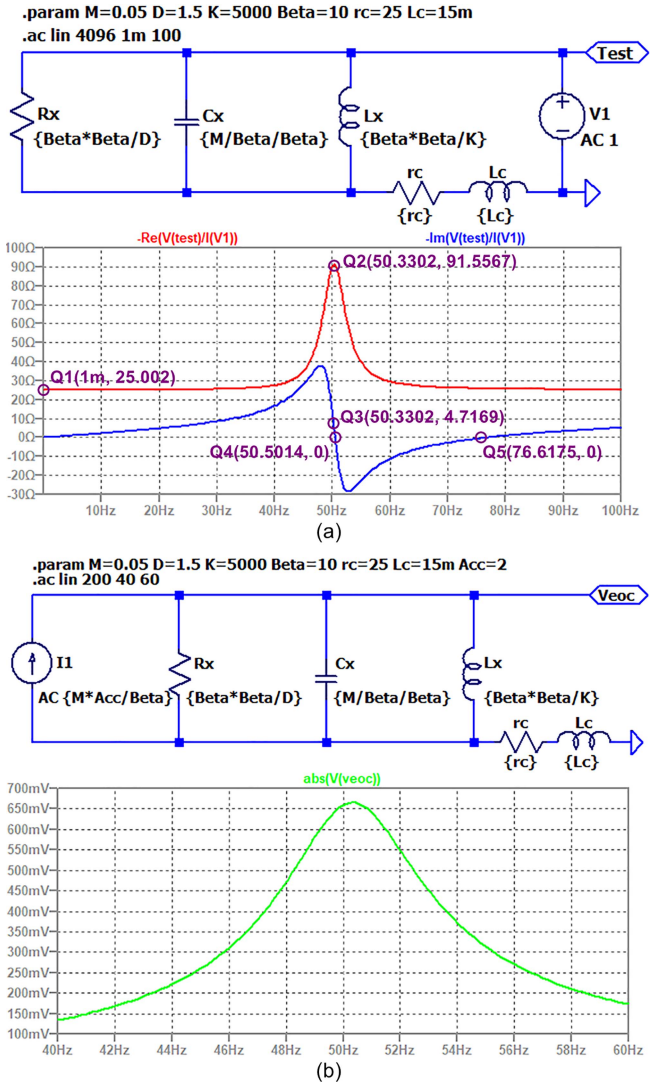

Fig. 7. (a) Simulation test of output impedance. (b) Simulation test of open-circuit voltage.

presented in Fig. 2(a). In the simulation, first, a 4096-point impedance sweep test of the circuit within a frequency range of 1 mHz–100 Hz is conducted. The curves of real part and imaginary part of the output impedance with five key points are plotted in Fig. 7(a). Second, a 200-point open-circuit voltage sweep test of the circuit within a frequency ranging from 40 to 60 Hz under an acceleration of 2 m/s^2 is performed, as plotted in Fig. 7(b). With the data of output impedance and open-circuit voltage, the proposed method can determine the parameters of the EMVEH successfully, as listed in Table III. The simulation test indicates that the proposed method has a high accuracy of parameter identification, and the relative error between determined values and simulated values is less than $\pm 1\%$.

The second simulation test is performed to investigate the effect of parameter errors on the performance estimation of linear EMVEHs. The open-circuit voltage of a linear EMVEH can be calculated by (7). According to resistive impedance

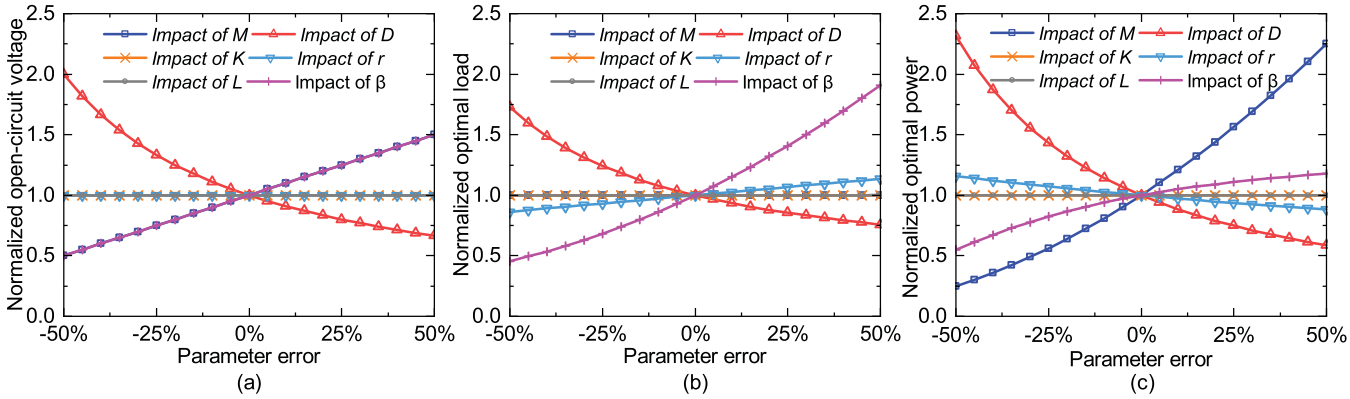

Fig. 8. (a) Normalized open-circuit voltage versus parameter error. (b) Normalized optimal load versus parameter error. (c) Normalized optimal power versus parameter error.

TABLE III
SIMULATION TEST RESULTS

Parameter	Simulated value	Determined value	Unit	Error*
ω_n	$50.3292 \times 2\pi$	$50.3302 \times 2\pi$	rad/s	+0.002%
ω_1	$50.5004 \times 2\pi$	$50.5014 \times 2\pi$	rad/s	+0.002%
ω_2	$76.6161 \times 2\pi$	$76.6175 \times 2\pi$	rad/s	+0.002%
ζ_m	0.047434	0.047379	—	−0.116%
k_e	1.154701	1.154637	—	−0.006%
M	50	50.1205	g	+0.241%
D	1.5	1.5019	N·s/m	+0.127%
K	5000	5012.2416	N/m	+0.245%
r	25	25.002	Ω	+0.008%
L	15	14.9159	mH	−0.561%
β	10	9.9836	N/A	−0.164%

*Error = Determined/Simulated−1.0.

TABLE IV
CORRELATION BETWEEN PERFORMANCE VARIATION AND PARAMETER ERROR

	Voltage	Load	Power
M	Positive, strong	Nearly uncorrelated	Positive, strong
D	Negative, strong	Negative, strong	Negative, strong
K	Uncorrelated	Nearly uncorrelated	Nearly uncorrelated
r	Uncorrelated	Positive, weak	Negative, weak
L	Uncorrelated	Nearly uncorrelated	Nearly uncorrelated
β	Positive, strong	Positive, strong	Positive, $\Delta\beta>0$: weak, $\Delta\beta<0$: strong

matching [31], [32], the optimal load resistance maximizing the power delivered to the load and the corresponding optimal output power can be obtained from (19) and (20), respectively. The simulated values of the six lumped parameters listed in Table III are used as baseline values. The baseline values of open-circuit voltage, optimal load, and optimal power are calculated from the baseline parameters under resonance conditions. By using the control variable method, only one parameter is changed and the other parameters are kept unchanged, and the corresponding open-circuit voltage, optimal load, and optimal power are recalculated. The calculated values are normalized with respect to the corresponding baseline values for a fair comparison. Therefore, the normalized baseline value is equal to 1.0, which is obtained when there are no parameter errors

$$R_{L,\text{opt}} = |Z_{\text{eq}}(\omega)| = \sqrt{(R(\omega))^2 + (X(\omega))^2} \tag{19}$$

$$P_{\text{opt}} = \frac{1}{2}\frac{|V_{\text{eq}}(\omega)|^2 R_{L,\text{opt}}}{(R(\omega) + R_{L,\text{opt}})^2 + (X(\omega))^2}. \tag{20}$$

Fig. 8 shows the impact of parameter errors on the performance variation of linear EMVEHs, which includes the normalized open-circuit voltage, normalized optimal load, and normalized optimal power. Parameter errors are measured as percentage deviations from baseline values and an observation range of −50% to +50% is selected. When the performance variation and parameter error have the same sign, it is defined as a positive correlation, otherwise, it is a negative correlation. In addition, when the performance variation reaches more than half of the parameter error, it is usually called strong correlation, otherwise, it is called weak correlation. Accordingly, the correlation between performance variation and parameter error can be concluded in Table IV. The difference between "uncorrelated" and "nearly uncorrelated" is that the performance variation of the former does not include the parameter error at all, while the performance variation of the latter includes the parameter error, but the corresponding impact is very small. In general, the estimation of output power of a linear EMVEH is of interest. According to the simulation results, the parameters M, D, and β have a strong impact on the normalized optimal power, and the parameter r has a weak impact, whereas the parameters L and K have almost no impact. Therefore, the identification accuracy of M, D, and β is critical to the performance estimation of linear EMVEHs.

V. TECHNICAL VALIDATIONS

A. Experimental Setup

To further verify the feasibility of the proposed method, experimental tests are carried out on two EMVEH prototypes, as demonstrated in Fig. 9(a). The first prototype (EMVEH-1) is a laboratory-built device, which is an unpackaged EMVEH. The second prototype (EMVEH-2) is a commercial device typed as VEG-30 from XIDAS IoT [29], which is a fully packaged EMVEH. Fig. 9(b) illustrates the experimental setup using an impedance analyzer to measure the output impedance of the prototype. Fig. 9(c) shows the experimental setup using a digital

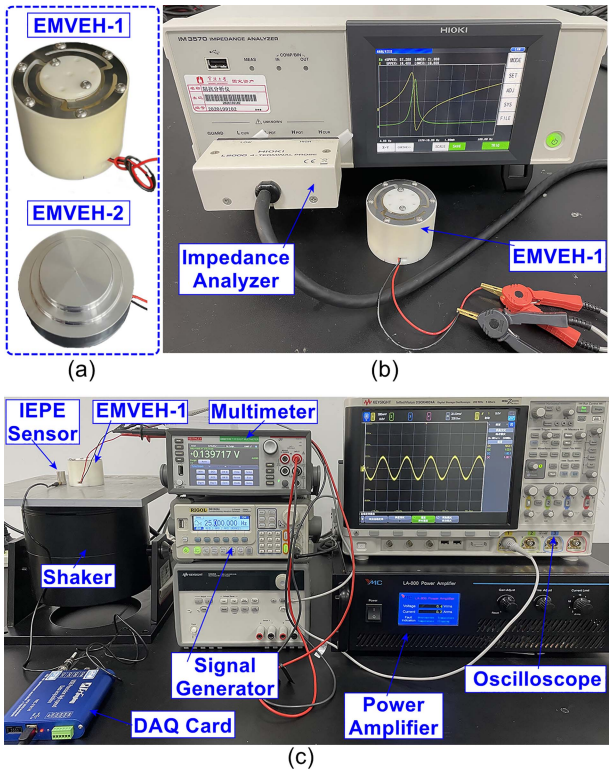

Fig. 9. (a) Two EMVEH prototypes. (b) Output impedance test setup. (c) Open-circuit voltage test setup.

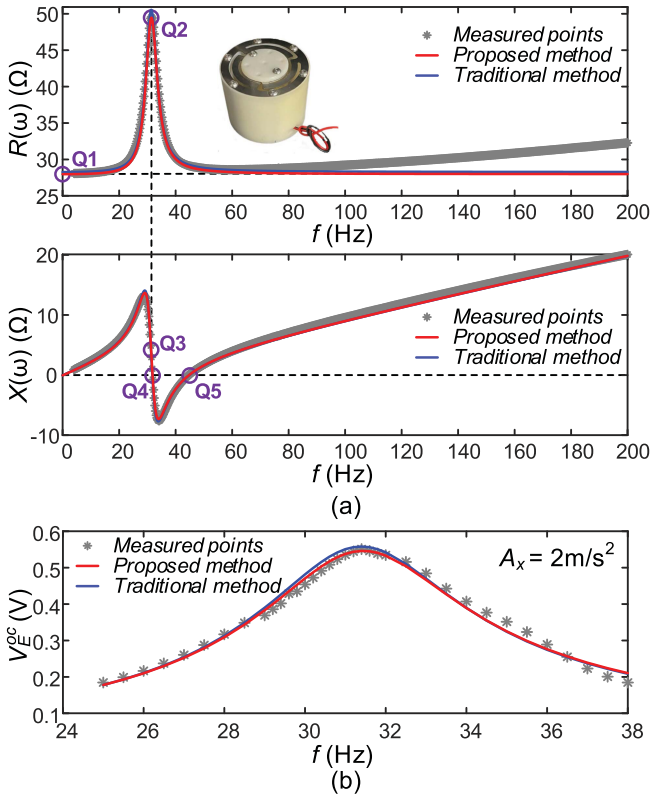

Fig. 10. Measurement results of EMVEH-1 prototype. (a) Real part $R(\omega)$ and imaginary part $X(\omega)$ of the output impedance versus frequency. (b) Open-circuit voltage $V_E^{\rm oc}$ versus frequency under 2 $\mathrm{m/s^2}$ acceleration.

multimeter to measure the open-circuit voltage of the prototype, which is also synchronously displayed on the oscilloscope. Meanwhile, the base acceleration is monitored by a commercial integrated electronics piezoelectric accelerometer in real-time. In addition, when the EMVEH has a large dynamic mass, the reaction force from the EMVEH may affect the working state of the shaker, especially near the resonance point, which may affect the measurement of base acceleration and open-circuit voltage. To minimize this effect, it is recommended to use a vibration shaker with negative feedback control or a stronger drive capability. Therefore, a strong vibration shaker (VT-500) with a weight of 30 kg and a peak driving force of 500 N is employed in the experiment.

B. Parameter Identification of EMVEH-1

Fig. 10(a) plots the real part $R(\omega)$ and imaginary part $X(\omega)$ of the output impedance of the EMVEH-1 prototype. Due to the capacity of the impedance analyzer IM3570, only an 801-point impedance sweep test within a frequency ranging from 4 to 200 Hz is conducted. Thus, the frequency resolution is 0.245 Hz in the impedance measurement. According to (11), the coil resistance r should be read from $R(0)$. Since the $R(\omega)$ curve gradually approaches a constant as the frequency decreases, the start point of 28.074 Ω at 4 Hz in the measurement, is simply taken as the coil resistance r.

As a comparison, the coil resistance r is measured to be 28.361 Ω in the pure dc test mode, and thus this approximation treatment only causes an error of -1.01%. The impact of this small error on performance estimation can be almost neglected according to the above simulation results. In addition, despite an error in r, it is still reasonable because the other parameters are independent and not affected by it. Then, based on the five key points Q_1–Q_5 located in Fig. 10(a), the values of ω_n, ζ_m, k_e, and L can be determined to be 31.440 × 2π rad/s, 0.07962, 1.0320, and 16.262 mH, respectively.

Fig. 10(b) also plots the measured open-circuit voltage of the EMVEH-1 prototype excited under an acceleration of 2 $\mathrm{m/s^2}$ within a frequency range of 25 to 38 Hz. There are a total of 36 measured points. According to (17), the value of β is resolved to 8.589 N/A. Then, the remaining parameters M, D, and K are calculated to 109.152 g, 3.433 N · s/m, and 4259.485 N/m, respectively. Since the EMVEH-1 prototype is an unpackaged device, its parameters can be also measured using the traditional method. Table V compares the parameter identification results of the traditional and proposed methods. It is observed that the parameters identified by the proposed method are close to that of the traditional method. The maximum deviation occurs in the damper coefficient D, and the relative error is only $+2.78\%$. Accordingly, this error can result in estimation errors of open-circuit voltage, optimal load, and optimal power under-estimates of 2.7%, 2.0%, and 3.4%, respectively.

In addition, the output impedance and open-circuit voltage of EMVEH-1 are reconstructed based on parameters identified by both methods, as shown by the red and blue solid-lines in Fig. 10.

TABLE V
DETERMINED PARAMETERS OF EMVEH-1

Parameter	Determined value		Error*
	Traditional Method	Proposed Method	
ω_n	$31.400 \times 2\pi$ rad/s	$31.440 \times 2\pi$ rad/s	+0.13%
ω_1	—	$31.830 \times 2\pi$ rad/s	—
ω_2	—	$44.625 \times 2\pi$ rad/s	—
ζ_m	0.07795	0.07962	+2.14%
k_e	1.0412	1.0320	−0.88%
M	108.6 g	109.152 g	+0.51%
D	3.340 N·s/m	3.433 N·s/m	+2.78%
K	4226.5 N/m	4259.485 N/m	+0.78%
r	28.361 Ω	28.074 Ω	−1.01%
L	16.221 mH	16.262 mH	+0.25%
β	8.621 N/A	8.589 N/A	−0.37%

*Error = Proposed/Traditional−1.0.

To estimate the goodness of reconstruction, the normalized root-mean-square error (NRMSE) is employed as given by

$$\text{NRMSE} = \frac{1}{p_{\max} - p_{\min}} \sqrt{\frac{\sum_{i=1}^{N} (\hat{p}_i - p_i)^2}{N}} \tag{21}$$

where N represents the number of data points. p_i and $\hat{p}_i$ are the ith measured and reconstructed points. $p_{\max}$ and $p_{\min}$ are the maximum and minimum points in the whole dataset, respectively. Accordingly, the NRMSE of $R(\omega)$, $X(\omega)$, and V_E^{oc} obtained based on the traditional method versus measured points are 0.0806, 0.0177, and 0.0486, respectively. The corresponding NRMSE between the proposed method and measured points are 0.0902, 0.0163, and 0.0370, respectively. The NRMSE of $R(\omega)$ is significantly larger than others, which is also reflected in Fig. 10(a). It can be seen that the error between the measured point of $R(\omega)$ and the reconstructed value based on both methods increases with increasing frequency. The underlying reason behind this is that the EMVEH-1 prototype is not a perfectly linear EMVEH. Therefore, this error is attributed to the limitations of the linear lumped parameter model rather than the proposed method. Overall, in the parameter identification of EMVEH-1, the proposed method is basically consistent with the traditional method in terms of both intuitive curves and quantitative data.

C. Parameter Identification of EMVEH-2

The EMVEH-2 prototype is a fully packaged device, which prevents the use of traditional methods. Thus, only the proposed method is performed on EMVEH-2. According to the provided datasheet, the nominal resonant frequency of EMVEH-2 is about 30 Hz [29]. First, an 801-point impedance sweep test within a frequency ranging from 4 to 200 Hz is conducted on EMVEH-2. However, since the EMVEH-2 prototype has a high mechanical quality factor (>60), this frequency resolution is insufficient in the critical region near its resonant point. Thus, an additional 801-point impedance sweep test in the 25–33 Hz range is added. Finally, Fig. 11 plots the measured results of output impedance and open-circuit voltage of EMVEH-2. The five key points Q_1–Q_5 are also clearly marked in Fig. 11(a). It can be observed that the positions of points Q_3 and Q_4 are very close. Therefore, this region actually requires high-frequency resolution. Fig. 11(b) plots the measured open-circuit voltage of

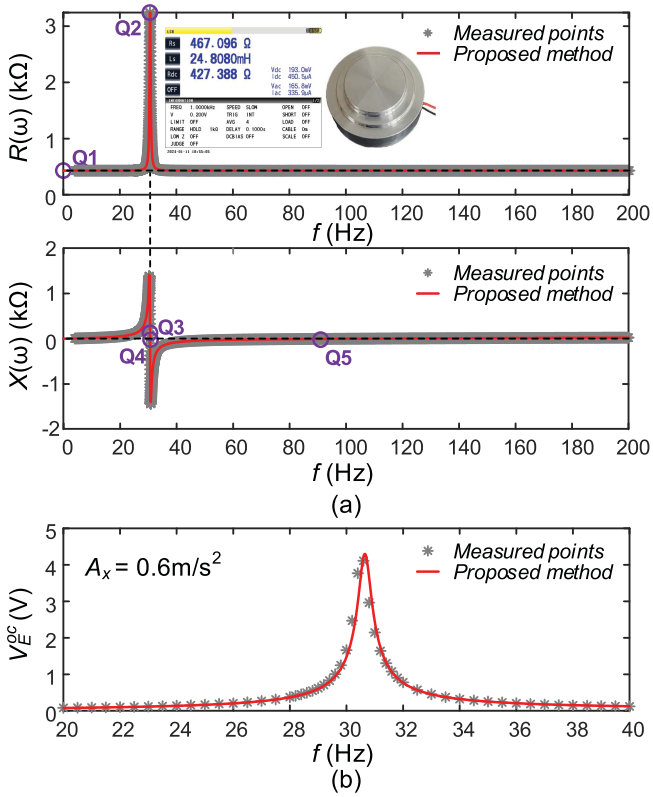

Fig. 11. Measurement results of EMVEH-2 prototype. (a) Real part $R(\omega)$ and imaginary part $X(\omega)$ of the output impedance versus frequency. (b) Open-circuit voltage V_E^{oc} versus frequency under 0.6 m/s^2 acceleration.

TABLE VI
DETERMINED PARAMETERS OF EMVEH-2

Parameter	Determined value		
	From Datasheet	Measurement	Proposed Method
ω_n	$30\times2\pi$ rad/s	—	$30.6500\times2\pi$ rad/s
ω_1	—	—	$30.6504\times2\pi$ rad/s
ω_2	—	—	$95.6023\times2\pi$ rad/s
ζ_m	—	—	0.00784
k_e	—	—	2.95456
M	—	—	55.1581 g
D	—	—	0.1665 N·s/m
K	—	—	2045.64 N/m
r	435 Ω	427.388 Ω	430.614 Ω
L	24 mH@1 kHz	24.808 mH@1 kHz	26.210 mH
β	—	—	21.634 N/A

the EMVEH-2 prototype excited under an acceleration of 0.6 m/s^2 within a frequency range of 20–40 Hz. There are a total of 53 measured points.

All the parameters are identified by the proposed method, as listed in Table VI. Then, the output impedance and open-circuit voltage of EMVEH-2 are reconstructed based on the determined parameters, as the red solid-lines plotted in Fig. 11. It is demonstrated that the reconstructed and measured results can reach a good agreement. In detail, the NRMSE of $R(\omega)$, $X(\omega)$, and V_E^{oc} obtained based on the proposed method versus measured points are 0.0030, 0.0028, and 0.0414, respectively. The small NRMSE values can confirm the goodness of reconstruction, as well as the parameters identified by the proposed method.

TABLE VII
TECHNICAL COMPARISON

Publication	Cheng et al. [21]	Elvin et al. [24]	Balato et al. [26]	Yuan et al. [27]	This work
Basic principle	Measurement based on physical definitions	Theoretical derivations with pre-tested data	Measurement based on optimal power	Simulation based on FEM analysis	Measurement based on Thevenin equivalent
Identifiable parameters	All	Some	All	None	All
Analytical solution	Yes	Yes	Yes	No	Yes
Required tests	Depends	Depends	Optimal power	None	Thevenin equivalent
Laser vibrometer	Required	Not required	Not required	Not required	Not required
Mechanical constraints	Required	Not required	Not required	Not required	Not required
Packaged EMVEH	Not applicable	Not applicable	Applicable	Not applicable	Applicable
NRMSE	—	—	—	—	$R(\omega)$, $X(\omega)$, V_E^{oc} Traditional Method: 0.0806, 0.0177, 0.0486 Proposed Method: 0.0902, 0.0163, 0.0370
Test accuracy in principle	High	Depends	High	Depends	High
Operation convenience	Complex	Complex	Complex	Simple	Simple

In addition, the datasheet shows that the typical coil resistance of EMVEH-2 is 435 Ω and the output impedance is 440 Ω with 24 mH at 1 kHz. However, they are nominal values for mass production and not specific to an individual. Due to manufacturing errors, there are uncertain differences between actual parameters and nominal values for each device. Based on direct LCR measurement, the measured coil resistance of EMVEH-2 is 427.388 Ω and the equivalent inductance is 24.808 mH at 1 kHz, as shown in Fig. 11(a). Based on the proposed method, the coil resistance and inductance are determined to be 430.614 Ω and 26.210 mH, respectively, and the relative errors are +0.75% and +5.65% as compared with the direct LCR measurement results. According to the above simulation results, the error of parameter L has almost no impact on the performance estimation of linear EMVEHs.

D. Technical Comparison

Table VII compares the proposed method with existing methods in terms of several technical characteristics. The lumped parameter identification process in [21] mainly adopts the traditional method according to the physical definitions of parameters. It usually requires laser vibrometers and mechanical constraints to construct specific test conditions, so it is not suitable for packaged EMVEHs. The method in [24] uses theoretical derivation instead of some experimental tests, but there is a relatively large test error if the formulas are not accurate enough. The method in [26] can determine all the lumped parameters according to the optimal output power without the need for laser vibrometers and mechanical constraints. However, the measurement of optimal output power requires traversing tests over a range of vibration frequencies and load resistances, which is complex. The method in [27] is a pure simulation method based on finite element analysis, and the result is only a lookup table, not an explicit electrical model. The proposed method relies on the Thevenin equivalent measurement of linear EMVEHs, which does not require laser vibrometers and mechanical constraints. Compared with the traditional method, this method has the same test accuracy and can be applied to the packaged EMVEHs and rapid measurement in industrial field.

VI. CONCLUSION

In this article, a new method based on Thevenin equivalent measurement and five-point extraction algorithm is proposed to identify the lumped parameters of a linear EMVEH. The required measurements only include the output impedance and open-circuit voltage. Also, the five-point extraction algorithm is analytical rather than simple curve fitting. The details of the method including theoretical derivations, proof of principle, comprehensive simulation, and experimental validations are fully presented, thereby substantiating the feasibility of the proposed method. Compared with the traditional method, the proposed method exhibits a maximum relative error of +2.78% in parameter D identification of an unpackaged laboratory-built EMVEH. In addition, this method can also work on a packaged commercial EMVEH and exhibits a maximum relative error of +5.65% in parameter L identification as compared with the direct LCR measurement results. Overall, the proposed method can offer high technical applicability, operation convenience, and test accuracy, which can be applied to industrial field measurement applications.

REFERENCES

[1] S. Roy, A. N. M. W. Azad, S. Baidya, M. K. Alam, and F. Khan, "Powering solutions for biomedical sensors and implants inside the human body: A comprehensive review on energy harvesting units, energy storage, and wireless power transfer techniques," *IEEE Trans. Power Electron.*, vol. 37, no. 10, pp. 12237–12263, Oct. 2022.

[2] J. Wang, Z. Chen, Z. Li, J. Jiang, J. Liang, and X. Zeng, "Piezoelectric energy harvesters: An overview on design strategies and topologies," *IEEE Trans. Circuits Syst., II, Exp. Briefs*, vol. 69, no. 7, pp. 3057–3063, Jul. 2022.

[3] C. Williams and R. Yates, "Analysis of a micro-electric generator for microsystems," *Sens. Actuators A Phys.*, vol. 52, no. 1, pp. 8–11, Mar. 1996.

[4] A. Karami, D. Galayko, and P. Basset, "A novel characterization method for accurate lumped parameter modeling of electret electrostatic vibration energy harvesters," *IEEE Electron Device Lett.*, vol. 38, no. 5, pp. 665–668, May 2017.

[5] W. Peng and S. Du, "The advances in conversion techniques in triboelectric energy harvesting: A review," *IEEE Trans. Circuits Syst. I, Reg. Papers*, vol. 70, no. 7, pp. 3049–3062, Jul. 2023.

[6] S. Roundy, "On the effectiveness of vibration-based energy harvesting," *J. Intell. Mater. Syst. Struct.*, vol. 16, no. 10, pp. 809–823, Oct. 2005.

[7] M. J. Guan and W. H. Liao, "On the equivalent circuit models of piezoelectric ceramics," *Ferroelectrics*, vol. 386, no. 1, pp. 77–87, Jan. 2009.

[8] J. Liang and W.-H. Liao, "Impedance modeling and analysis for piezoelectric energy harvesting systems," *IEEE/ASME Trans. Mechatron.*, vol. 17, no. 6, pp. 1145–1157, Dec. 2012.
[9] Q. Cai and S. Zhu, "Unified strategy for overall impedance optimization in vibration-based electromagnetic energy harvesters," *Int. J. Mech. Sci.*, vol. 165, Jan. 2020, Art. no. 105198.
[10] S. M. Hoseyni, A. Aghakhani, and I. Basdogan, "Experimental admittance-based system identification for equivalent circuit modeling of piezoelectric energy harvesters on a plate," *Mech. Syst. Signal Proc.*, vol. 208, Feb. 2024, Art. no. 111016.
[11] Y. Tan, Y. Dong, and X. Wang, "Review of MEMS electromagnetic vibration energy harvester," *J. Microelectromech. Syst.*, vol. 26, no. 1, pp. 1–16, Feb. 2017.
[12] D. Zhu, S. Roberts, T. Mouille, M. J. Tudor, and S. P. Beeby, "General model with experimental validation of electrical resonant frequency tuning of electromagnetic vibration energy harvesters," *Smart Mater. Struct.*, vol. 21, no. 10, Sep. 2012, Art. no. 105039.
[13] Y. Li, J. Li, A. Yang, Y. Zhang, B. Jiang, and D. Qiao, "Electromagnetic vibrational energy harvester with microfabricated springs and flexible coils," *IEEE Trans. Ind. Electron.*, vol. 68, no. 3, pp. 2684–2693, Mar. 2021.
[14] H. Sun et al., "An optimized design of compact self-powered module based on electromagnetic vibration energy harvester considering engineering feasibility," *IEEE Trans. Ind. Appl.*, vol. 59, no. 1, pp. 767–778, Jan./Feb. 2023.
[15] X. Wang, X. Liang, Z. Hao, H. Du, N. Zhang, and M. Qian, "Comparison of electromagnetic and piezoelectric vibration energy harvesters with different interface circuits," *Mech. Syst. Signal Proc.*, vol. 72/73, pp. 906–924, May 2016.
[16] J. Leicht and Y. Manoli, "A 2.6 μW-1.2 mW autonomous electromagnetic vibration energy harvester interface IC with conduction-angle-controlled MPPT and up to 95% efficiency," *IEEE J. Solid-State Circuit*, vol. 52, no. 9, pp. 2448–2462, Sep. 2017.
[17] M. Balato, L. Costanzo, and M. Vitelli, "MPPT in wireless sensor nodes supply systems based on electromagnetic vibration harvesters for freight wagons applications," *IEEE Trans. Ind. Electron.*, vol. 64, no. 5, pp. 3576–3586, May 2017.
[18] H. Xiao, H. Peng, X. Liu, and H. Sun, "Fully self-powered inductorless electromagnetic vibration energy harvesting system using auxiliary coils for hysteresis current MPPT control," *IEEE Trans. Power Electron.*, vol. 37, no. 11, pp. 13192–13204, Nov. 2022.
[19] Z. Feng, H. Peng, and Y. Kang, "Complex impedance matching for electromagnetic vibration energy harvesting: Key parameters and low power consumption implementation," *IEEE Trans. Power Electron.*, vol. 38, no. 12, pp. 15659–15670, Dec. 2023.
[20] H. Xiao, H. Peng, H. Sun, Y. Zhao, X. Liu, and C. Jiang, "Automatic impedance matching with dual time-scale P&O in fully self-powered electromagnetic vibration energy harvesting," *IEEE Trans. Power Electron.*, vol. 39, no. 3, pp. 3377–3390, Mar. 2024.
[21] S. Cheng, N. Wang, and D. P. Arnold, "Modeling of magnetic vibrational energy harvesters using equivalent circuit representations," *J. Micromechanics Microengineering*, vol. 17, no. 11, Nov. 2007, Art. no. 2328.
[22] E. Arroyo and A. Badel, "Electromagnetic vibration energy harvesting device optimization by synchronous energy extraction," *Sens. Actuators, A*, vol. 171, no. 2, pp. 266–273, Nov. 2011.
[23] G. Poulin, E. Sarraute, and F. Costa, "Generation of electrical energy for portable devices: Comparative study of an electromagnetic and a piezoelectric system," *Sens. Actuators A Phys.*, vol. 116, no. 3, pp. 461–471, Oct. 2004.
[24] N. G. Elvin and A. A. Elvin, "An experimentally validated electromagnetic energy harvester," *J. Sound Vib.*, vol. 330, no. 10, pp. 2314–2324, May 2011.
[25] E. Arroyo, A. Badel, F. Formosa, Y. Wu, and J. Qiu, "Comparison of electromagnetic and piezoelectric vibration energy harvesters: Model and experiments," *Sens. Actuators A Phys.*, vol. 183, pp. 148–156, Aug. 2012.
[26] M. Balato, L. Costanzo, and M. Vitelli, "Resonant electromagnetic vibration harvesters: Determination of the equivalent electric circuit parameters and simplified closed-form analysis for the identification of the optimal diode bridge rectifier DC load," *Int. J. Elect. Power Energy Syst.*, vol. 84, pp. 111–123, Jan. 2017.
[27] C. Yuan, D. Hohlfeld, and T. Bechtold, "Towards system-level simulation of an electromagnetic energy harvester model via equivalent circuit extraction from ANSYS maxwell 3D," in *2023 24th Int. Conf. Thermal, Mech. Multi-Phys. Simul. Experiments Microelectronics Microsystems*, Apr. 2023, pp. 1–5.
[28] L. Hayes, "Product spotlight - PMG17 vibration energy harvester," *IEEE Control Syst. Mag.*, vol. 28, no. 1, pp. 107–108, Feb. 2008.
[29] Xidas-IoT, "Vibration-based energy-harvesting generator," 2024. Accessed: Jul. 18, 2024. [Online]. Available: https://www.mouser.in/pdfDocs/Xidas_VEG_DS.pdf
[30] T. T. Toh, S. W. Wright, and P. D. Mitcheson, "Resonant frequency tuning of an industrial vibration energy harvester," *J. Phys.: Conf. Ser.*, vol. 557, no. 1, Nov. 2014, Art. no. 012128.
[31] N. Kong, D. S. Ha, A. Erturk, and D. J. Inman, "Resistive impedance matching circuit for piezoelectric energy harvesting," *J. Intell. Mater. Syst. Struct.*, vol. 21, no. 13, pp. 1293–1302, Sep. 2010.
[32] S.-W. Wang, Y.-W. Ke, P.-C. Huang, and P.-H. Hsieh, "Electromagnetic energy harvester interface design for wearable applications," *IEEE Trans. Circuits Syst., II, Exp. Briefs*, vol. 65, no. 5, pp. 667–671, May 2018.

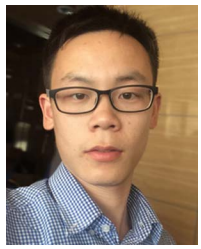

Huakang Xia received the B.E. degree in aircraft design and engineering and the Ph.D. degree in measuring and testing technologies and instruments from the Nanjing University of Aeronautics and Astronautics, Nanjing, China, in 2012 and 2017, respectively.

He is currently an Associate Professor with the Faculty of Electrical Engineering and Computer Science, Ningbo University, Ningbo, China. His research interests include energy harvesting systems, ultralow power circuit design, embedded systems, and motor control techniques.

Yinshui Xia received the B.S. degree in physics and the M.E. degree in electronic engineering from Hangzhou University, Hangzhou, China, in 1984 and 1991, respectively, and the Ph.D. degree in electronic engineering from Edinburgh Napier University, Edinburgh, U.K., in 2003.

He was a Visiting Scholar with King's College London, London, U.K., in 1999, and then joined Edinburgh Napier University as a Research Assistant and Enterprise Fellow from 2000 to 2005. He is currently a Professor with the Faculty of Electrical Engineering and Computer Science, Ningbo University, Ningbo, China. His research interests include low-power digital circuit design, logic synthesis and optimization, and SoC design.

Libo Qian (Member, IEEE) received the B.S. degree in electron mechanics and the M.S. and Ph.D. degrees in microelectronics from Xidian University, Xi'an, China, in 2007, 2010, and 2013, respectively.

From 2013 to 2022, he was an Associate Professor with the Faculty of Electrical Engineering and Computer Science, Ningbo University, Ningbo, China. He is currently a Professor with the Key Laboratory of Analog Integrated Circuits, and Hangzhou Institute of Technology, Xidian University. His research interests include energy harvesting integrated circuits and high-efficiency power integrated circuits design.

Ge Shi (Senior Member, IEEE) received the B.E. degree in electrical engineering and automation and the M.E. degree in detection technology and automation from China Jiliang University, Hangzhou, China, in 2004 and 2010, respectively, and the Ph.D. degree in micro-nano information system from Ningbo University, Ningbo, China, in 2018.

He is currently a Professor with China Jiliang University. His current research interests include energy harvesting systems, sensors and measuring technology, ultralow power integrated circuit design, and embedded systems.

Zhidong Chen received the B.E. degree in electronic and information engineering and the M.S. degree in electronic circuit and system from Hangzhou Dianzi University, Hangzhou, China, in 2011 and 2014, respectively, and the Ph.D. degree in micro-nano information system from Ningbo University, Ningbo, China, in 2022.

He is currently a Lecturer with Zhejiang Wanli University, Ningbo, China. His research interests include energy harvesting systems, sensors, and measuring technology.

Xiudeng Wang (Member, IEEE) received the B.E. degree in communication engineering, the M.E. degree in electronic circuits and systems, and the Ph.D. degree in electronic science and technology from Ningbo University, Ningbo, China, in 2016, 2019, and 2023, respectively.

Since 2023, he has been an Associate Professor with the Key Laboratory of Analog Integrated Circuits, and Hangzhou Institute of Technology, Xidian University, Xi'an, China. His current research interests include energy harvesting technologies, sensor and measurement technologies, power management, and energy-efficient integrated circuits.